An Optimized CSS-ISAC Signal Design for Localization with LEO Satellites

Daniel Egea-Roca, José A. López-Salcedo, Gonzalo Seco-Granados
Dpt. of Telecommunications and Systems Engineering, IEEC-CERES, UAB, Spain
{daniel.egea, jose.salcedo, gonzalo.seco}@uab.es

***Abstract*—Integrated sensing and communications (ISAC) is expected to play a key role in developing many innovative applications. This is the case for localization systems when operating from low Earth orbit (LEO). For example, it has been studied that global navigation satellite systems (GNSSs) need alternative waveform configurations when moving to LEO. These new waveforms must allow both sensing and communication functions for localization purposes. In this sense, a chirp spread spectrum (CSS) signal is shown in the literature to be a good option for LEO localization with reduced complexity with respect to current configurations. For this reason, in this paper, we propose an optimized CSS-ISAC signal design for LEO localization. The proposed signal design is shown with numerical results to provide a flexible way to optimize useful ISAC performance trade-offs with reduced signal processing complexity.**

***Index Terms*—CSS, ISAC, Localization, LEO.**

I. Introduction

Integrated sensing and communications (ISAC) has been identified as a key enabler for 6G [1], but its extent reaches applications beyond classical radar sensing and communication networks. This is the case of localization systems in which we need to sense time delay and Doppler to provide measurements that allow us to compute the position of the user [2]. Furthermore, to make this localization possible the reception of some information is needed such as the position of the anchor nodes, some corrections (e.g., clock and atmospheric errors), or time references. It is here where we find the link between localization and ISAC systems.

A clear example is global navigation satellite systems (GNSS) that uses satellites as anchor nodes to transmit signals that allow the users on Earth to compute its position [2]. The last trend is to move GNSS to low Earth orbit (LEO) to exploit the opportunities that LEO may bring to localization. These opportunities deal with the main challenges of current localization systems [3]–[5], but they also bring some important challenges that need to be solved. For localization, the most critical aspect is related to the higher Doppler frequency in LEO compared to current systems [6]. This compromises the performance and most importantly it complicates the acquisition process of the received signals [7].

A chirp spread spectrum (CSS) signal has been proposed in the last years to provide ISAC capabilities for LEO localization with reduced complexity compared to current settings [5], [8]–[10]. This fact shows that waveform design plays an important role in localization and therefore ISAC systems. The focus is to define a dual-function waveform that is capable of sensing and communication (S&C) by the shared use of signaling resources [1]. Depending on the integration level, ISAC waveforms are classified in the literature as non-overlapped resource allocation [11]–[13] and fully unified waveforms. The maximum integration gain in ISAC is obtained by the second approach.

Fully unified ISAC waveforms are generally designed according to three different philosophies [14], [15]: sensing- or communication-centric design, and joint design. The two first options aim at incorporating the communication or sensing functionality into existing sensing or communication waveforms, respectively. This limits the performance of one of the S&C functionalities, which can be solved by considering a joint design as done in this paper. The goal of a joint design is to provide an ISAC waveform specifically designed to jointly provide S&C instead of relying on existing sensing and communication configurations [1]. To do so, a weighting factor is used to balance the priority/preference assigned to S&C functionalities in the waveform design.

In this paper, we consider a CSS signal design for ISAC to be used in LEO localization. The use of CSS-ISAC waveform design has barely been adopted only for sensing-centric designs [1], thus without fully exploiting the integration gain. The CSS signal design for LEO localization targeting low-complexity is studied in [5], [8]–[10], but without considering any performance trade-off. Based on this observation, we propose in this paper an optimized CSS-ISAC joint design useful for localization with LEO satellites. In particular, the contribution of this paper is to provide a joint design of CSS targeting the optimization of a valuable S&C performance trade-off. To do so, we introduce in Section II the considered ISAC system model used in Section III and Section IV to analyze the proposed ISAC performance and to explain the proposed signal design, respectively. Finally, Section V gives the numerical results and Section VI concludes this paper.

II. CSS-ISAC LEO Localization

In this section, we introduce the model for the ISAC system with CSS used in this paper. This will include the general CSS signal model and its corresponding S&C model. For the S&C part, we describe the considered signal model as well as its receiver processing in terms of estimation and

This work was partly supported by the Catalonia NewSpace Strategy, the Spanish R+D project under Grant PID2020-118984GB-I00, and by the ICREA Academia Program.

978-8-3503-8544-1/24/$31.00 ©2024 IEEE

data demodulation. Furthermore, we will consider the multiple satellite access to provide ISAC capabilities from different satellites in view in a LEO constellation, thus considering the multiple satellite interference (MSI).

A. Signal Model

Let us consider the most general form of a CSS waveform, which is a signal that linearly varies its frequency. This variation can be positive (up-chirp) or negative (down-chirp) within a given bandwidth B and during a given duration or chirp period, $T_{\rm c}$. This variation is characterized by the *chirp rate* or slope of the CSS signal defined as $\mu \doteq B/T_{\rm c}$ so that the baseband frequency of the CSS signal is given by

$$f_{\pm}(t; f_0) = \pm f_{\mu}(t; f_0) \doteq \pm \left([f_0 + \mu t]_B - B/2 \right), \quad (1)$$

with $f_0 \in [0, B]$ the initial frequency, the $\pm$ sub-index denotes an up- or down-chirp, and $f_{\mu}(t) \in [-B/2, B/2]$ by the application of the modulus-B operator (i.e., $[\cdot]_B$).

Since each baseband chirp is bandlimited to $B/2$, it can be sampled at $F_{\rm s} = B$ with $N_{\rm c} = BT_{\rm c}$ samples at each chirp period. Let $f_{\mu}[n] = f_{\mu}(t)|_{t=n/F_{\rm s}}$ be the sampled baseband frequency, and $\phi_{\mu}[n]$ its corresponding phase. Then, the up-chirp signal samples are written in this paper as

$$s_{\mu}[n; f_0] = e^{j\phi_{\mu}[n]} \doteq \exp\left(j2\pi \sum_{k=0}^{n-1} f_{\mu}[k; f_0] \right), \quad (2)$$

and the down-chirp corresponds to its complex conjugate, i.e., $s^*_{\mu}[n; f_0]$. In this paper, when $f_0 = 0$ we will write $s_{\mu}[n]$. This is the case of the *sensing component*, which only focuses on estimating the sensing parameters given by $\boldsymbol{\theta}_{\rm s} \doteq [\tau, f_{\rm D}]^{\top}$, with τ and $f_{\rm D}$ the (normalized by $1/F_{\rm s}$) time-delay and corresponding Doppler frequency experienced after propagation through the channel.

Once the sensing parameters are estimated we use them to synchronize the *communication component* at the receiver to demodulate the delivered data denoted by $\theta_{\rm d}$. In this paper, we consider the S&C components can be independently processed at the receiver to obtain the desired parameters. Let $\boldsymbol{\theta} = \{\boldsymbol{\theta}_{\rm s}, \theta_{\rm d}\}$ be either the sensing or communication parameters so that the received samples are written as

$$r[n; \boldsymbol{\theta}] = \sqrt{P_{\rm s}} \cdot s_{\mu,\boldsymbol{\theta}}[n] + w[n], \quad (3)$$

with $P_{\rm s}$ the received signal power, $\{s_{\mu,\boldsymbol{\theta}_{\rm s}}[n], s_{\mu,\theta_{\rm d}}[n]\}$ the received signal component for either sensing or communication, respectively, and $w[n]$ AWGN with power σ_w^2. The metric $\text{CN0} \doteq B \cdot (P_{\rm s}/\sigma_w^2)$ will be henceforth referred to as the carrier-to-noise density ratio (CN0).

B. Sensing Signal Model

To jointly estimate the time delay and Doppler frequency, we need the transmission of an up- and down-chirp together as done in [5], [16], [17]. This signal will be considered here for the sensing, and it will be henceforth referred to as the BOK-chirp signal. Recall the up-chirp is the complex conjugate of the down-chirp so that we write

$$s_{\mu,\boldsymbol{\theta}_{\rm s}}[n] = \sqrt{\frac{1}{2}} \left(e^{j\phi_{\mu}[n-\tau]} + e^{-j\phi_{\mu}[n-\tau]} \right) e^{j2\pi f_{\rm D}(n-\tau)}, \quad (4)$$

and the received signal is given by (3). This signal structure allows us to obtain the sensing parameters applying the so-called *de-chirp process* to each up- and down-chirp component [5].

Let $r_{\text{dc},\pm}[n] \doteq r[n] \cdot \exp\left(\mp j\phi_{\mu}[n]\right)$ be the de-chirped signal and $R_{\text{dc},\pm}(f)$ its discrete-time Fourier transform (DFT) at the continuous frequency f. Then, the de-chirped frequency used for the sensing parameter estimation is defined as

$$f_{\text{dc}\pm} \doteq \arg\max_f \left\{ \Re\left\{ R_{\text{dc}\pm}(f) \right\} \right\}, \quad (5)$$

with $\Re\{\cdot\}$ the real part operator. The maximum likelihood estimate (MLE) of $\boldsymbol{\theta}_{\rm s}$ is given by [5], [18]

$$\widehat{\boldsymbol{\theta}}_{\rm s} = \left[-\frac{f_{\text{dc}+} - f_{\text{dc}-}}{2\mu}, \frac{f_{\text{dc}+} + f_{\text{dc}-}}{2} \right]^{\top}. \quad (6)$$

Note that $\widehat{\tau} \in \pm T_{\rm c}/2$ and $\widehat{f}_{\rm D} \in \pm B/2$, thus fixing the time-delay and Doppler frequency values we can measure without ambiguity.

C. Communication Signal Model

Once the sensing parameters are estimated, we can synchronize the received signal so that $\tau = f_{\rm D} = 0$ for the communication signal model. The use of different initial frequencies as data modulation is used in this paper, and it will be henceforth referred to as FSK-CSS. For its definition, let $N_{\rm b}$ be the number of bits per symbol, and $M = 2^{N_{\rm b}}$ be the number of symbols in an M-ary constellation. Then, the k-th symbol with $k = 1, 2, \ldots, M$ assigns the following initial frequency $f_k = k(B/M) \in (0, B]$. Now, let $\theta_{\rm d} = f_k$ so that $s_{\mu,\theta_{\rm d}}[n] = \sqrt{0.5}(s_{\mu}[n; \theta_{\rm d}] + s^*_{\mu}[n; \theta_{\rm d}])$ and the received as in (3). Then, the data can be demodulated as the second element of $\widehat{\theta}_{\rm s}$ in (6), i.e., $\widehat{\theta}_{\rm d} = |\widehat{\theta}_{\rm s}|_2$.

D. Multiple Satellite Access

Localization with $N_{\rm sat}$ LEO satellites is considered in this paper. For this purpose, we need the reception of at least 4 satellites to obtain the position of a user [2]. We consider different transmission slopes from different satellites given by μ_i for $i = 1, 2, \ldots, N_{\rm sat}$. Also, let $\boldsymbol{\theta}_i = \{\boldsymbol{\theta}_{\rm s}^{(i)}, \theta_{\rm d}^{(i)}\}$ be the S&C parameters of the i-th satellite, respectively, and $\boldsymbol{\theta} = [\boldsymbol{\theta}_1, \boldsymbol{\theta}_2, \ldots, \boldsymbol{\theta}_{N_{\rm vis}}]$ with $N_{\rm vis}$ the number of visible satellites given by the set $\mathcal{I}_{\rm vis} = \{k_1, k_2, \ldots, k_{N_{\rm vis}}\}$. Then, each satellite generates its own signal component $s_{\mu_i,\boldsymbol{\theta}}[n]$ following the previous S&C signal models and experiencing different propagation conditions $\boldsymbol{\theta}_{\rm s}^{(i)} = \{\tau_i, f_{\rm D}^{(i)}\}$. So that

$$r[n; \boldsymbol{\theta}] = \sqrt{P_{\rm s}} \sum_{i \in \mathcal{I}_{\rm vis}} s_i[n; \boldsymbol{\theta}_i] + w[n]. \quad (7)$$

Now, let $R^{(i)}_{\text{dc}\pm}(f)$ be the DFT of the i-th de-chirped signal, and $\mathcal{H}_j$ with $j = \{1, 0\}$ the hypothesis that the i-th satellite is

visible or not, respectively. Then, $\mathcal{I}_{\text{vis}}$ is identified by resorting to the following GLRT [19] for $i = 1, \ldots, N_{\text{sat}}$:

$$T_i(\mathbf{x}) = \Re\left\{ R^{(i)}_{\text{dc}+}(f_{\text{dc}+}) + R^{(i)}_{\text{dc}-}(f_{\text{dc}-}) \right\} \underset{\mathcal{H}_0}{\overset{\mathcal{H}_1}{\gtrless}} h, \quad (8)$$

where h is the detection threshold. Then, the corresponding S&C estimator is applied for all detected satellites. It is important to note that the reception of different signals affects the performance in terms of detection, estimation, and demodulation.

Now, let $\rho_i[n] = \exp(-j\phi_{2\mu_i}[n])$ be the interference between up- and down-chirp components in the received BOK-chirp, and $\rho_{zi}[n] = \exp(-j\phi_{\mu_i+\mu_z}[n]) + \exp(-j\phi_{\mu_i-\mu_z}[n])$ be the interference of satellite z into the i-th received signal. By the spread spectrum nature of CSS, these interferences are modeled as pseudorandom noise so that they contribute to an increment of the noise power quantified by the MSI component given by

$$\sigma_i^2 = 2 \cdot \frac{P_{\text{s}}}{N_{\text{c}}} \sum_{n=0}^{N_{\text{c}}} \Re\left\{ \rho_i[n] + \sum_{\substack{z \in \mathcal{I}_{\text{vis}} \\ z \neq i}} \rho_{zi}[n] \right\}^2. \quad (9)$$

This increment of the noise power has to be included in the received CN0 in the form of carrier-to-noise density plus interference ratio (CIN0) defined as

$$\text{CIN0} \doteq \text{CN0}\left(1 + \text{CN0} \cdot (\sigma_i^2/B)\right)^{-1} \quad (10)$$

III. ISAC Performance Analysis

For the joint design of ISAC waveforms, it is of paramount importance to derive S&C key performance indexes (KPIs) to define valuable trade-offs for the optimization of the ISAC signal design. It is worth saying that MSI plays a key role in the definition of KPIs since it links both S&C metrics. In other words, a reduction of the MSI leads to improved performance for both S&C functionalities. Henceforth, the MSI effects are considered by relying on the CIN0 defined in (10). We consider the results for a given satellite so that the sub-index i will be henceforth removed.

A. Sensing Performance

Sensing performance metrics are based on detection and estimation metrics. Two KPIs are considered in this paper: the sensitivity defined as the capability to detect a given signal, and the accuracy on the estimated parameters.

1) Sensitivity: The capability of the GLRT detector $T(\mathbf{x})$ to detect a signal is measured by the probabilities of detection (PD) and false alarm (PFA):

$$\begin{aligned} P_{\text{D}}(h) &\doteq \Pr\left\{ T(\mathbf{x}) \geq h \mid \mathcal{H}_1 \right\}, \\ P_{\text{FA}}(h) &\doteq \Pr\left\{ T(\mathbf{x}) \geq h \mid \mathcal{H}_0 \right\}. \end{aligned} \quad (11)$$

To derive a closed-form expression, let $Z \doteq T(\mathbf{x}) = X_+ + X_-$ with $X_\pm \doteq \arg\max_f\{Y_{f\pm}\}$ and $Y_{f\pm}$ the DFT frequency bins after applying the $\Re\{\cdot\}$ operator. So, Z and $Y_{f\pm}$ are linked by the $\max_f\{\cdot\}$ operator. Thus, the distribution of Z is driven by the *total* probability of N_{c} *cells* distributed as $Y_{f\pm}$.

Now, let $\sigma_{\text{T}}^2 = \sigma_w^2 + \sigma_i^2$ with σ_i^2 given in (9), CIN0 given in (10), and $Q(\cdot)$ the Q-function. Then, based on the link between total and cell probabilities [20] with the AWGN model in Section II-A the PD and PFA can be computed as

$$\begin{aligned} P_{\text{FA}}(h, T_{\text{c}}) &= 1 - \left(1 - Q\left(\frac{h}{\sqrt{2N_{\text{c}}\sigma_{\text{T}}^2(T_{\text{c}})}}\right)\right)^{N_{\text{c}}}, \\ P_{\text{D}}(h, T_{\text{c}}) &= Q\left(\frac{h}{\sqrt{2N_{\text{c}}\sigma_{\text{T}}^2(T_{\text{c}})}} - \sqrt{2T_{\text{c}}\text{CIN0}(T_{\text{c}})}\right). \end{aligned} \quad (12)$$

We have emphasized the dependence of T_{c} in parenthesis on PD, PFA, the MSI power, and CIN0. This result is very useful from the signal and receiver design point of view as it will be shown in Section IV.

2) Ranging accuracy: For a theoretical evaluation of the sensing parameters estimation, we base on the Cramér-Rao Bound (CRB) of the estimated parameter for the considered signal model. To do so, since the sensing parameters are un-coupled when using the BOK-chirp, the CRB of $(\widehat{f}_{\text{D}})$ $\widehat{\tau}$ can be derived from the signal model given by (4) when assuming (τ) $f_{\text{D}} = 0$. So, the derivation of CRB_τ is reduced to the derivation of the CRB from the signal model in (3) when considering the signal in (2) and $f_{\text{D}} = 0$. After some straightforward calculus, we get (e.g. from (3.37) in [18])

$$\text{CRB}_{\widetilde{\tau}}(T_{\text{c}}) = \frac{3}{(2\pi)^2 B^2 T_{\text{c}} \text{CIN0}(T_{\text{c}})}. \quad (13)$$

Note we use the $\widetilde{\tau}$ index to indicate the s^2 units of the CRB.

B. Communication Performance

Communication performance metrics are based on efficiency and reliability. We will consider the bit error rate (BER) and data rate, which are introduced next. These two KPIs are selected because of it usefulness in localization systems. Spectral efficiency is another efficiency metric used in communications, but it is not considered as KPI for localization.

1) Bit error rate: For the evaluation of the reliability of the communication, we rely on the BER of the FSK-CSS signal considered in this paper. To show the dependence of this BER on the signal design parameters, it is useful to look at closed-form expressions based on curve fitting, or BER approximations as in [21]:

$$P_{\text{e}}(T_{\text{c}}, M) = 0.5 \cdot Q\left(\sqrt{2\text{CIN0}(T_{\text{c}}) \cdot T_{\text{c}}} - \zeta(M)\right), \quad (14)$$

with $\zeta(M) = \sqrt{1.386 \cdot \log_2(M) + 1.154}$. In this paper, for the sake of ISAC, we keep T_{c} as a degree of freedom for the signal design.

2) Data rate: To quantify the amount of data we can transmit with a given signal configuration, we compute the number of bits transmitted per chirp period:

$$R_{\text{b}}(T_{\text{c}}, M) \doteq \frac{\log_2(M)}{T_{\text{c}}} = \frac{N_{\text{b}}}{T_{\text{c}}}. \quad (15)$$

We consider this data rate more convenient for a joint design than the channel capacity, although some ISAC literature has considered the capacity as KPI to be traded-off with some sensing metric [1].

The reason for using data rate instead of capacity is that we are targeting a joint design for ISAC. This is the reason that we kept $T_{\rm c}$ as a degree of freedom to optimize some performance. Then, M will be fixed as the maximum possible value that satisfies some signal design constraints (e.g., BER constraint) as done in Section IV. Note this is different from the traditional signal design for communications, in which all the signal design parameters are chosen to optimize the communication performance. Is in this case that we can think about achieving the channel capacity, but this may not be the case in ISAC.

IV. Optimized Joint CSS-ISAC Signal Design

This section proposes a joint design of a CSS signal for ISAC. This design includes the selection of the CSS signal parameters that drive the performance in terms of S&C. In this paper, we consider these parameters to be $\boldsymbol{\theta}_{\rm SD} \doteq [T_{\rm c}, M]^\top$. Other parameters involved in the ISAC performance and driving the selection of $\boldsymbol{\theta}_{\rm SD}$ are classified as *input* and *constraints* parameters. The former are usually limited in practice so we do not have a degree of freedom to select them. In our case, these parameters include $\boldsymbol{\theta}_{\rm in} \doteq [B, {\rm CN0}]^\top$. The constraint parameters include those requirements to be considered during the signal design. We consider requirements in terms of PFA, PD, and BER given by $\boldsymbol{\theta}_{\rm c} \doteq [\alpha, \beta, \gamma]^\top$, respectively. With this setting, in this section we first introduce the general formulation of the proposed signal design, and then we consider two different trade-offs.

A. Constrained Signal Design Optimization

The ultimate target of a joint design is to optimize some KPI of interest for ISAC, usually contradictory. For instance, for sensing we would like to optimize the ranging accuracy, whereas for communications we would like to maximize the data rate. Separate optimization processes would drive to large $T_{\rm c}$ for sensing, but short $T_{\rm c}$ for communication. For this reason, it is important to define valuable S&C performance trade-offs for an optimal selection of $\boldsymbol{\theta}_{\rm SD}$ in terms of ISAC. Based on the previous setting, we consider $\boldsymbol{\theta}_{\rm in}$ as deterministic (given) known parameters and we use the signal design constraints in $\boldsymbol{\theta}_{\rm c}$ to bound the domain of $\boldsymbol{\theta}_{\rm SD}$.

To show the general framework used for the ISAC signal design proposed in this paper, let h_α be the detection threshold that satisfies the PFA constraint as $h_\alpha = \{h : P_{\rm FA}(h, T_{\rm c}) = \alpha\}$. Also, let $\mathcal{T}_\beta = \{T : P_{\rm D}(h_\alpha, T) \geq \beta\}$ and $\mathcal{M}_\gamma(T) = 2^{\mathcal{X}_\gamma(T)}$ with $\mathcal{X}_\gamma(T) = \{x \in \mathbb{N} : P_{\rm e}(T, 2^x) \leq \gamma\}$ be the set of chirp periods and constellation sizes that satisfy the sensitivity and BER constraint, respectively. Then, the signal design parameters will be selected so that $T_{\rm c} \in \mathcal{T}_\beta$ and $M \in \mathcal{M}_\gamma(T_{\rm c})$. Furthermore the constellation size will be selected as the maximum $M \in \mathcal{M}_\gamma(T_{\rm c})$, which can be numerically solved:

$$M^*(T_{\rm c}) = \max_{M \in \mathcal{M}_\gamma(T_{\rm c})} \{M \in \mathbb{N} : M \leq N_{\rm c}\}, \tag{16}$$

With this set of $\boldsymbol{\theta}_{\rm SD}$ we can define a valuable performance trade-off useful for the optimal design of the signal design parameters. This trade-off is denoted by a function $\{T_{\rm c}, M\} \rightarrow f(T_{\rm c}, M)$ and its constrained optimization as

$$T_{\rm c} = \arg \min_{T \in \mathcal{T}_\beta} \{f\left(T, M^*(T)\right)\}. \tag{17}$$

with $M^*(T)$ as in (16).

B. Complexity minimization

We focus here on minimizing the receiver complexity as considered in [8].

$$\mathcal{C}(T_{\rm c}) = 8 \cdot BT_{\rm c}\left(1 + \log_2(BT_{\rm c})\right). \tag{18}$$

Then, the goal is to find the shortest chirp period possible that satisfies $T_{\rm c} \in \mathcal{T}_\beta$. Note the data demodulation complexity considered in this paper does not depend on M. This is why the complexity is independent of M, which is selected as in (16) when $T_{\rm c}$ is fixed after the minimization of $\mathcal{C}(T_{\rm c})$. The optimization problem in this case becomes

$$T_{\rm cs} = \arg \min_{T_{\rm c} \in \mathcal{T}_\beta} \{\mathcal{C}(T_{\rm c})\} = \arg \min_{T_{\rm c} \in \mathcal{T}_\beta} \{T_{\rm c} : BT_{\rm c} \in \mathbb{N}\}. \tag{19}$$

In other words, $T_{\rm cs}$ is given by the minimum chirp period that satisfies the sensitivity requirements and it produces an integer number of samples $N_{\rm c} = BT_{\rm c}$. To find $T_{\rm cs}$, let

$$\eta\left(T_{\rm c}\right) = \left[Q^{-1}\left(1 - (1-\alpha)^{1/N_{\rm c}}\right) - Q^{-1}\left(\beta\right)\right]^2, \tag{20}$$

with CIN0 in (10). Then, $T_{\rm cs}$ can be numerically solved as

$$T_{\rm cs} = \frac{\eta\left(T_{\rm cs}\right)}{2{\rm CIN0}(T_{\rm cs})}. \tag{21}$$

C. ISAC performance maximization

The previous optimization does not consider KPIs as ranging accuracy and data rate, they are fixed by the minimum chirp period. Nevertheless, better performances can be achieved by leveraging on larger $T_{\rm c}$ values at the expense of increasing the complexity. Note, that larger $T_{\rm c}$ values than the minimum one will also satisfy the design constraints. Different approaches can be considered to obtain this larger $T_{\rm c}$ based on different ISAC performance trade-offs [1]. We consider here a joint design to provide an optimized ISAC waveform by using a weighting factor $\rho \in [0, 1]$ to balance the weight assigned to S&C functionalities in the signal design.

In other words, ρ and $1 - \rho$ denote the priority/preference for the S&C performance in the ISAC system, respectively. In particular, the following trade-off is considered:

$$f(T_{\rm c}, M^*) = \rho \cdot {\rm CRB_d}(T_{\rm c}) + (1-\rho)\frac{2a}{R_{\rm b}\left(T_{\rm c}, M^*\right)}, \tag{22}$$

with $a = 10^{-3}$, ${\rm CRB_d}$ in meters, $R_{\rm b}$ computed as in (15) and $M^* = M^*(T_{\rm c})$ given by (16). The value of a is fixed to

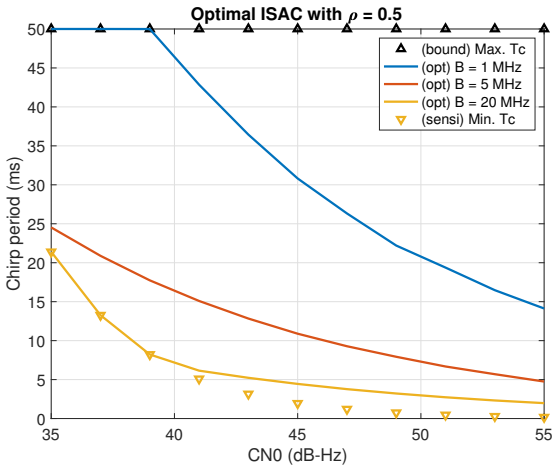

Fig. 1. Chirp period for the optimized ISAC design as a function of CN0 for $\rho = 0.5$. The results for the minimum chirp period and the maximum considered bound are also shown as a reference.

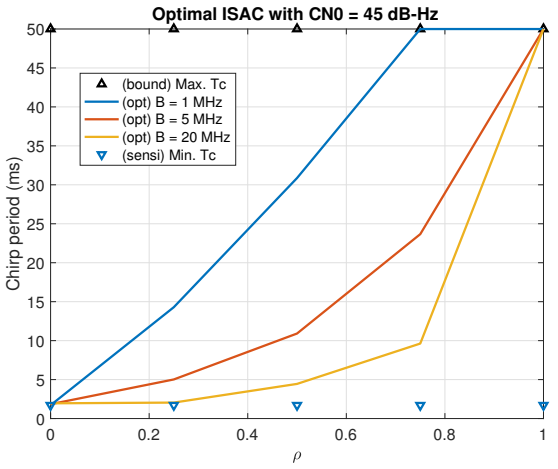

Fig. 2. Chirp period for the optimized ISAC design as a function of ρ for CN0$=45$ dB-Hz. The results for the minimum chirp period and the maximum considered bound are also shown as a reference.

keep S&C performances with the same order of magnitude. Otherwise, the convergence of the optimization process to a global minimum is compromised. We have also considered a time-multiplexing scheme for the S&C components, therefore the factor two in the data rate. Then, the optimized chirp period can be numerically solved as

$$T_{\mathrm{c}}^{*} = \arg \min_{T \in \mathcal{T}_{\beta}} f(T, M^{*}(T)). \tag{23}$$

V. Numerical Results

In this section, we show the numerical results for the design processes and performance analysis previously studied. To do so, we will first obtain the optimized chirp period given by (21) and (23) and their corresponding constellation size given by (16). Second, we will compute the corresponding sensing and communication performance metrics given by the CRB and data rate computed as in (13) and (15), respectively. For the computation of the optimized chirp periods, we rely on the *fminbnd* MATLAB function using a maximum chirp period of $T_{\max} = 50$. To obtain the constellation size we also rely on the *fminbnd* and we use the *berawgn* MATLAB function to compute the BER of an FSK modulation.

For the computation of the results, we need the value of CIN0 for different T_{c} values. We numerically compute the CIN0 by generating the corresponding interference signal samples as described in Section II-D. We consider $N_{\mathrm{vis}} = 25$ visible satellites among the total $N_{\mathrm{sat}} = 100$ satellites in the constellation. The interference results for 10^3 different sets of visible satellites are averaged to produce the MSI in (9), which is fed in (10) to produce the CIN0 values. The different slopes μ_i are generated as the multi-dual slope (MDS) scheme in [8]. We provide numerical results for different $\boldsymbol{\theta}_{\mathrm{in}} \doteq [B, \mathrm{CN0}]^{\top}$ relevant for localization with LEO. Finally, for the constrained optimization we consider $\boldsymbol{\theta}_{\mathrm{c}} \doteq [\alpha, \beta, \gamma] = [10^{-5}, 0.95, 10^{-3}]$.

With this framework, we first show in Fig. 1 the optimized chirp period for different CN0 values, $\rho = 0.5$ and $B = \{1, 5, 20\}$ MHz. We also include the upper bound given by $T_{\max}$, and T_{cs} is used here as a lower bound. The results show how the ISAC optimized chirp period decreases when either the CN0 or the bandwidth increases. An interesting result of Fig. 1 is the behavior of the optimized chirp period for different bandwidth values. For *high* bandwidth values, we have $T_{\mathrm{c}}^{*} = T_{\mathrm{cs}}$ until some CN0 value for which $T_{\mathrm{c}}^{*} > T_{\mathrm{cs}}$. For example, in Fig. 1 and $B = 20$ MHz we get $T_{\mathrm{c}}^{*} = T_{\mathrm{cs}}$ for CN0$\leq$ 39 dB-Hz. This contrasts with *small* bandwidth values, which produces $T_{\mathrm{c}}^{*} = T_{\max}$ for small CN0 values and $T_{\mathrm{cs}} < T_{\mathrm{c}}^{*} < T_{\max}$ otherwise. For instance, in Fig. 1 and $B = 1$ MHz gives $T_{\mathrm{c}}^{*} = T_{\max}$ for CN0$\leq$ 39 dB-Hz.

The reason for this result is that for a high-bandwidth regime and low CN0, the optimal approach is to be favorable in terms of data rate by fixing $T_{\mathrm{c}}^{*} = T_{\mathrm{cs}}$ and using the available bandwidth to increase M. In this case, the quality of the channel is too bad to get a good CRLB. On the other hand, when the quality of the channel improves (i.e., high CN0) and it allows for improved accuracy, the optimal approach is to be favorable in terms of CRB by increasing T_{c}. This increase in T_{c} can be compensated in this case by increasing M thanks to the improvements in CN0 in the high-CN0 regime. This last behavior also applies to the case of a low-bandwidth regime, independently of the CN0 value.

A similar behavior is experienced in Fig. 2, which shows similar results but when $\mathrm{CN0} = 45$ dB-Hz and different values of $\rho \in [0, 1]$ are used. For the same reasons as before, for high bandwidth values $T_{\mathrm{c}}^{*} = T_{\mathrm{cs}}$ for small ρ values to be favorable for data rate and $T_{\mathrm{c}}^{*} \to T_{\mathrm{cs}}$ as ρ increases (this being beneficial for CRLB). The shorter bandwidth value the smaller ρ value is needed for the convergence. Furthermore, from Fig. 2 we see that the optimal design can be tuned with the selection of ρ: with $\rho = 0$ we obtain a short chirp period given by T_{cs} to be favorable in terms of (communication) data rate, whereas with $\rho = 1$ we get a large chirp period to be favorable in terms of (sensing) CRLB. Intermediate ρ values provide intermediate

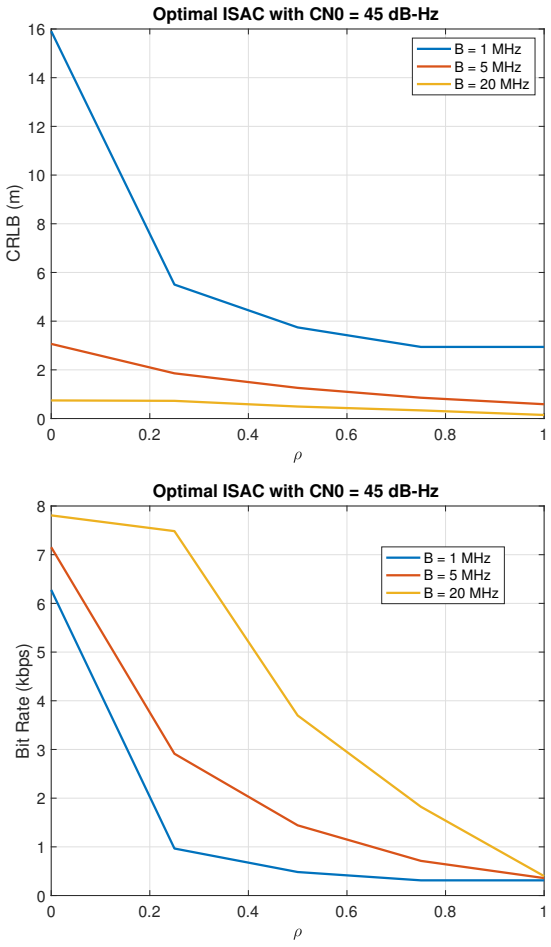

Fig. 3. Optimal ISAC performance as a function of ρ and CN0$=45$ dB-Hz: (Up) CRLB and (down) data rate results

chirp periods and trade-offs between S&C KPIs.

Finally, the previous conclusions are translated into the corresponding KPIs as shown in Fig. 3: the best data rate (i.e., >6 kbps depending on bandwidth) is obtained with $\rho=0$ but giving the worst ranging accuracy (i.e., 16 m for $B=1$ MHz). The best-ranging accuracy is obtained for $\rho=1$ with values <4 m for all considered bandwidths and tens of centimeters for $B\geq 5$ MHz. In this case, though, we get the worst simulated data rate around 0.5 kbps. From these results, it is interesting to see that even the extreme cases of $\rho=0$ and $\rho=1$ produce good performance results in terms of CRB and data rate, respectively. As an example, the current GPS L1 C/A signal provides a ranging accuracy of tens of meters but with a data rate of 50 bps [2].

VI. Conclusions

This paper has proposed a joint design for ISAC with a CSS signal useful for LEO localization. The proposed signal design targets the optimization of useful ISAC performance trade-offs. This optimization provides useful signal design parameters $\{T_c, M\}$ for given input parameters $\{B, \text{CN0}\}$ and constraints in terms of sensitivity and BER. Moreover, this optimal design includes in its signal model the effects of interference between satellites. So, the design parameters as other waveform parameters such as the chirp slope are optimally fixed to reduce interference and improve the ISAC performance. Two optimization options have been considered: the complexity and the trade-off between CRB and data rate. However, we have provided a general framework to be used for any optimization target. Based on the provided results we prove the capability of the proposed design to tune the S&C performance with the weighting factor ρ. An interesting conclusion from the results is that complexity can be optimized together with the performance trade-off only for wide-band signals and low signal conditions or for communication-oriented systems (i.e., $\rho=0$). Otherwise, the complexity must be increased to optimize the performance trade-off. Future work can follow from the general framework provided in this paper. For instance, spectral efficiency or other performance metrics might be included into the optimization process. Different useful S&C trade-offs could be also considered. Finally, more accurate signal models can be considered to include into the optimization process the effects of HW limitations/impairments, environmental impact, etc. So, the proposed general optimization framework in this paper opens an interesting research line on CSS-ISAC signal design.

References

[1] F. Liu, Y. Cui, C. Masouros, J. Xu, T. X. Han, Y. C. Eldar, and S. Buzzi, "Integrated Sensing and Communications: Toward Dual-Functional Wireless Networks for 6G and Beyond," *IEEE Journal on Selected Areas in Communications*, vol. 40, no. 6, pp. 1728–1767, 2022.

[2] D. Egea-Roca, M. Arizabaleta-Diez, T. Pany, F. Antreich, J. A. Lopez-Salcedo, M. Paonni, and G. Seco-Granados, "GNSS user technology: State-of-the-art and future trends," *IEEE Access*, vol. 10, pp. 39 939–39 968, 2022.

[3] Z. Qu, G. Zhang, H. Cao, and J. Xie, "LEO satellite constellation for Internet of things," *IEEE Access*, vol. 5, pp. 18 391–18 401, aug 2017.

[4] O. Kodheli, A. Guidotti, and A. Vanelli-Coralli, "Integration of satellites in 5G through LEO constellations," in *Proc. IEEE Global Communications Conference (GLOBECOM)*, jul 2017, pp. 1–6.

[5] D. Egea-Roca, J. A. López-Salcedo, G. Seco-Granados, and E. Falletti, "Comparison of several signal designs based on chirp spread spectrum (CSS) modulation for a LEO PNT system," in *Proc. 34th International Technical Meeting of the Satellite Division of the Institute of Navigation (ION GNSS+)*, sep 2021, pp. 2804–2818.

[6] A. H. Irfan, N. Al-Dhahir, and J. E. Hershey, "Doppler characterization for LEO satellites," *IEEE T. Commun.*, vol. 46, no. 3, pp. 309–313, 1998.

[7] X. Li, L. Chen, B. Xu, and C. Zhang, "Study on the method of fast acquisition in LEO satellite DSSS communication system," in *Proc. IEEE Int. Conf. on Electronic Measurement and Instruments (ICEMI)*, 2011, pp. 325–328.

[8] D. Egea-Roca, J. Lopez-Salcedo, G. Seco-Granados, and E. Falletti, "Performance analysis of a multi-slope chirp spread spectrum signal for PNT in a LEO constellation," in *Proc. 10th IEEE Workshop on Satellite Navigation Technology (NAVITEC)*, 2022.

[9] D. Egea-Roca, J. A. López-Salcedo, and G. Seco-Granados, "Performance Analysis of the Pilot- and Data-Component of a CSS Signal for LEO-PNT," *Eng. Proc.*, pp. 1–9, 2023.

[10] ——, "On The Complexity of Non-Coherent Acquisition of Chirp Spread Spectrum Signals," in *IEEE International Conference on Acoustics, Speech, and Signal Processing Workshops (ICASSPW)*, 2023, pp. 1–5.

[11] H. Wymeersch, G. Seco-Granados, G. Destino, D. Dardari, and F. Tufvesson, "5G mmwave positioning for vehicular networks," *IEEE Wireless Communications*, vol. 24, no. 6, pp. 80–86, 2017.

[12] M. Bica and V. Koivunen, "Radar waveform optimization for target parameter estimation in cooperative radar-communications systems," *IEEE Transactions on Aerospace and Electronic Systems*, vol. 55, no. 5, pp. 2314–2326, 2019.

[13] F. Liu, C. Masouros, A. Li, H. Sun, and L. Hanzo, "MU-MIMO Communications with MIMO Radar: From Co-Existence to Joint Transmission," *IEEE Transactions on Wireless Communications*, vol. 17, no. 4, pp. 2755–2770, 2018.

[14] D. Ma, N. Shlezinger, T. Huang, Y. Liu, and Y. C. Eldar, "Joint Radar-Communication Strategies for Autonomous Vehicles: Combining Two Key Automotive Technologies," *IEEE Signal Processing Magazine*, vol. 37, no. 4, pp. 85–97, 2020.

[15] J. A. Zhang, F. Liu, C. Masouros, R. W. Heath, Z. Feng, L. Zheng, and A. Petropulu, "An Overview of Signal Processing Techniques for Joint Communication and Radar Sensing," *IEEE Journal on Selected Topics in Signal Processing*, vol. 15, no. 6, pp. 1295–1315, 2021.

[16] Y. Qian, L. Ma, and X. Liang, "Symmetry chirp spread spectrum modulation used in LEO satellite internet of things," *IEEE Commun. Lett.*, vol. 22, no. 11, pp. 2230–2233, nov 2018.

[17] A. B. Martinez, A. Kumar, M. Chafii, and G. Fettweis, "A chirp-based frequency synchronization approach for flat fading channels," in *Proc. 2nd IEEE 6G Wireless Summit: Gain Edge for the 6G Era*, mar 2020.

[18] S. M. Kay, *Fundamentals of Statistical Signal Processing, Volume 1: Estimation Theory*. Prentice Hall Upper Saddle River, NJ, USA, 1998.

[19] ——, *Fundamentals of Statistical Signal Processing, Volume 2: Detection Theory*. Prentice Hall Upper Saddle River, NJ, USA, 1998.

[20] D. Borio, L. Camoriano, and L. L. Presti, "Impact of GPS acquisition strategy on decision probabilities," *IEEE T. Aero. Elec. Sys.*, vol. 44, no. 3, pp. 996–1011, 2008.

[21] T. Elshabrawy and J. Robert, "Closed-Form approximation of LoRa modulation BER performance," *IEEE Commun. Lett.*, vol. 22, no. 9, pp. 1778–1781, sep 2018.